Granular Matter (2018) 20:12
https://doi.org/10.1007/s10035-017-0780-z

ORIGINAL PAPER

The influence of rolling resistance on the stress-dilatancy and fabric anisotropy of granular materials

Yiming Liu[1] · Huabei Liu[1] · Haijun Mao[2]

Received: 5 April 2017 / Published online: 8 January 2018

Abstract
The effects of rolling resistance on the stress-dilatancy behavior and fabric anisotropy of granular materials were investigated through a three-dimensional discrete element method (DEM). A rolling resistance model was incorporated into the DEM code PFC3D and triaxial DEM simulations under simulated drained and undrained conditions were carried out. The results show that there existed a threshold value of the rolling friction. When the rolling friction was smaller than this value, the mechanical behavior of granular materials under both drained and undrained conditions were substantially influenced by the rolling friction, but the influence diminished when it was larger than the threshold value. A linear relationship has been observed between the dilatancy coefficient and the natural logarithm of the rolling-friction coefficient when it was smaller than the threshold value. An increase in the rolling friction led to an increase in the fabric anisotropy of all strong contacts under both testing conditions until the threshold value was attained. The investigation on the effect of rolling friction on the microstructure of granular materials revealed that the rolling friction enhanced the stability of force chains, which resulted in the difference in the stress-dilatancy behavior. Finally, the relationship between the stress ratio q/p' and the fabric measure at strong contacts H_d^s/H_m^s was found independent of the inter-particle friction, rolling friction and testing conditions.

Keywords Discrete element method · Rolling resistance · Dilatancy · Fabric anisotropy · Granular materials

1 Introduction

Granular materials are inherently discontinuous, anisotropic, nonlinear, and multi-scaled [25,64], resulting in very complex behavior. To fully understand this complexity, studies on the mechanical behavior of granular materials have been focused on the behavior at different scales. Recently, the influence of the basic particle properties on the behavior of granular materials has attracted considerable attentions in the research community. Among the various characteristics, particle shape plays an essential role and should be comprehensively investigated. Over the past few decades, extensive experimental studies have been performed to clarify the effects of particle shape on the mechanical behavior of granular materials, including the shear strength, dilatancy, crushability, shear-induced localization, and instability [12,15,21,23,50,55,61]. However, it is difficult to quantitatively relate the morphology of realistic particles to the mechanical behavior of granular materials by experimental tests.

An alternative approach is by means of the discrete element method (DEM), which is pioneered by Cundall and Strack [16] and has been widely used in various research fields. Utilizing DEM, different options have been proposed to study the particle-shape effects of granular materials. Hosn et al. [1] summarized these options into three categories. One category is by using particles with complex shapes, such as ellipses and polygons in two-dimensional (2D) or ellipsoids and polyhedrons in three dimensional (3D) analyses [30,40,42]. However, such complex shapes were reported to be computationally expensive in detecting contacts and calculating forces and torques. The second category

✉ Huabei Liu
hbliu@hust.edu.cn

Yiming Liu
yiming_liu@hust.edu.cn

Haijun Mao
hjmao@whrsm.ac.cn

[1] School of Civil Engineering and Mechanics, Huazhong University of Science and Technology, 1037 Luoyu Road, Wuhan 430074, Hubei, China

[2] Institute of Rock and Soil Mechanics, Chinese Academy of Sciences, Xiaohongshan, Wuhan 430071, Hubei, China

is by using clumps or cluster, but the accurate characterization and modeling of realistic particle shape may still encounter computational challenges [66]. In contrast, the rolling-resistance model is an alternative to simulate particle-shape effects [2,7,29,32,33,41]. Conventional DEM assumes point-to-point contacts among particles, which may lead to excessive rolling that does not exist in most granular materials. To overcome this limitation, contact constitutive model considering rolling resistance was developed in order to resist the free rotation of particles [29]. Extensive numerical and theoretical studies have shown that rolling-resistance model is able to reflect the particle-shape effects [19,20,59,60].

Previous results have shown that rolling resistance can significantly affect the macro mechanical behavior of granular materials, such as the shear strength [9,29,31,37,64–66], the development of shear band [37,51], the capability to resist liquefaction [64,66], and the force and fabric anisotropies [24,28,54]. However, ambiguities still exist in the literature, one of which is the effect of the rolling friction on the stress-dilatancy response. Most results showed that the dilatancy angle increased with an increase in the rolling-friction coefficient, while Plassiard et al. [44] showed that the dilatancy of granular materials was independent of the rolling friction. Furthermore, the mechanism of the effect of rolling resistance on the stress-dilatancy relationship is still not clear. Another fundamental issue that should be thoroughly addressed is the influence of rolling resistance on the micro properties of granular materials. Although considerable efforts have been devoted to tackle this issue [24,28,54], the effect of rolling resistance on the relationship between the micro and macro responses is still not clear.

This study investigated the effects of the rolling friction on the dilatancy and fabric anisotropy of granular materials by conducting 3D discrete-element analyses. A rolling-resistance model was incorporated into the DEM code PFC3D [27]. A series of numerical tests were carried out under simulated drained and undrained conditions, and the stress–strain relationships under both conditions were presented and compared with previous results. Then, the relationship between the rolling friction and the stress-dilatancy behavior was fully investigated. The evolution of the microstructure and the relationship between the micro and macro quantities considering both the rolling-friction effect and testing condition were also explored.

2 DEM simulations

2.1 Rolling-resistance model

In recent years, the effect of rolling resistance on the micro and macro mechanical behavior has been investigated by many investigators. According to Ai et al. [2], four different categories of rolling-resistance models are commonly used in DEM:

Type A: Models in this category apply a pair of constant torques on each pair of particles in a contact to represent the rolling friction. The torque acts in a direction opposite to the rolling direction. A typical model of this type is defined as [67]:

$$M_r = -f_r r F_n \frac{\omega_{vel}}{|\omega_{vel}|} \tag{1}$$

where f_r is the coefficient of rolling friction, F_n is the contact normal force, and ω_{vel} is the relative angular velocity of the two particles in contact. r is defined as follows:

$$r = 2\frac{r^A r^B}{r^A + r^B} \tag{2}$$

where r^A and r^B are the radii of the two contacting particles, respectively.

Type B: The torque in this type of models is related to both the contact normal force and the relative angular velocity. This model can be expressed as:

$$M_r = -f_r r F_n \left(\omega_i r_i - \omega_j r_j\right) \tag{3}$$

where $\omega_i r_i - \omega_j r_j$ represents the relative translational velocity induced by rolling at the contact.

Type C: This model was initially defined by Iwashita and Oda [29] and refined by Wang and Gutierrez [58] and Ai et al. [2]. The total rolling resistant torque M_r consists of a spring torque M_{rk} and a viscous damping torque M_{rd} in this model. The spring torque M_{rk} is defined in an incremental way by the following equation:

$$\mathrm{M}^k_{r,t+\Delta t} = \begin{cases} \mathrm{M}^k_{r,t} - k_r \omega_{rel} \Delta t \text{ provided that } \left|\mathrm{M}^k_{r,t} - k_r \omega_{rel} \Delta t\right| < f_r r \left|F_n\right| \\ f_r r \left|F_n\right| \dfrac{\mathrm{M}^k_{r,t} - k_r \omega_{rel} \Delta t}{\left|\mathrm{M}^k_{r,t} - k_r \omega_{rel} \Delta t\right|} \text{ otherwise} \end{cases} \tag{4}$$

where k_r is the rolling stiffness, Δt is a timestep in the discrete-element analysis. The viscous damping torque M_{rd} is of the form of:

$$\mathrm{M}^v_{r,t+\Delta t} = \begin{cases} -C_r \omega_{rel} \text{ provided that } \mathrm{M}^v_{r,t+\Delta t} < f_r r \left|F_n\right| \\ 0 \quad \text{otherwise} \end{cases} \tag{5}$$

where the damping rate, C_r, is defined as a proportion of the critical damping; $C_r = \zeta 2\sqrt{k_r I_r}$ with I_r being the equivalent moment of inertia.

The rolling resistance model proposed in this study is modified from Type C.

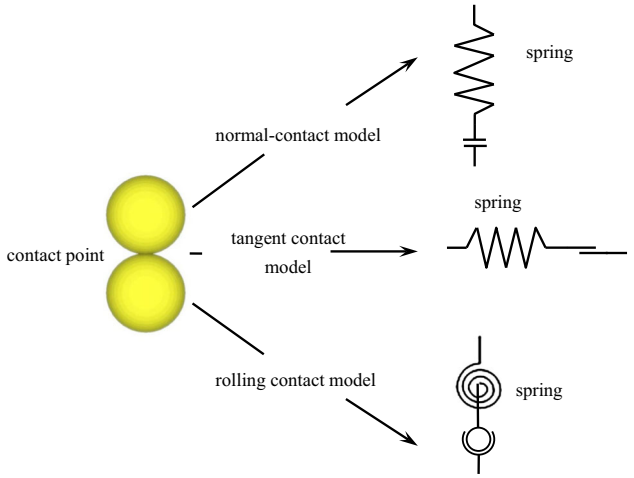

Fig. 1 Rolling resistance model. Reproduced with permission from Belheine et al. [9]

Type D: This type of model applies a resistive torque that is independent of the contact between particles. It tends to apply a resistive torque that is related to the angular velocity of each individual particle rather than the relative behavior of a pair of contacting particles [59].

To take into account the particle-shape effects of granular materials, a user-defined rolling-resistance model was incorporated into PFC3D. The rolling-resistance contact model between two contacting particles, as shown in Fig. 1, is composed of three components, which represent the mechanical behavior in the normal, tangential, and rolling directions, respectively.

For the normal and tangential components, the built-in linear contact model is adopted to represent the force-displacement behavior between contacting particles. The normal and shear forces are given by:

$$F_i^n = K^n u_i^n \tag{6}$$

$$\Delta F_i^s = -K^s \Delta u_i^s \tag{7}$$

where F_i^n and u_i^n denote the contact force and normal displacement in the normal direction, ΔF_i^s and Δu_i^s are the incremental force and displacement in the tangential direction, K^n is the normal stiffness, and K^s is the tangential stiffness. Considering that the springs of the two contacting spheres act in series, K^n and K^s are defined by the following equations:

$$K^n = \frac{k_n^A k_n^B}{k_n^A + k_n^B} \tag{8}$$

$$K^s = \frac{k_s^A k_s^B}{k_s^A + k_s^B} \tag{9}$$

where k_n and k_s are the normal and tangential stiffness values of the contacting spheres, respectively, in which the superscripts A and B denote the two spheres in contact.

The constitutive behavior tangential to the particle contact is bounded by a slip model, which is defined by the friction coefficient μ at the contact. The slip model is mobilized at contact i when the following condition is satisfied:

$$\left|F_i^s\right| \geq \mu \left|F_i^n\right| \tag{10}$$

where F_i^s and F_i^n are the contact shear and normal forces, respectively.

The new rolling component consists of an elastic spring and a roller. A contact moment M_i at the contact plane is added to resist the relative rotation between two particles. The rolling resistance moment M_i can be written as:

$$M_i = k_r \theta_r \tag{11}$$

where θ_r is the relative rolling vector between two particles, and k_r is the rolling stiffness and its value is obtained as [7]:

$$k_r = 2r F_i^n J_n \tag{12}$$

where J_n is the rolling-stiffness coefficient. Based on the initial definition, J_n varies theoretically from 0.25 to 0.5 [7]. The value of J_n depends on the nature of the contact. A more rigid contact leads to a higher value. Since perfectly-rigid spherical particles were used in this study, J_n takes the value of 0.5. The influence of this parameter will also be discussed in this study. r is defined by Eq. (2).

The roller against rolling is mobilized when M_i exceeds a value of $f_r r F_i^n$:

$$|M_i| \geq f_r r F_i^n \tag{13}$$

2.2 Numerical triaxial-compression tests

In order to investigate the effect of rolling resistance on the mechanical behavior of granular materials, a series of numerical tests were carried out under both simulated drained and undrained conditions. All the test specimens were generated based on the radii expansion method [27]. Each sphere was firstly created and randomly positioned inside a cylindrical space, and then it was expanded to its finial size and cycled to equilibrium. The numerical specimen was encircled by a cylindrical wall and two loading plates, which had a height of 6.0 m and a diameter of 3.0 m as shown in Fig. 2a. The ratio between H/D was 2.0 based on the dimension requirements of actual conventional triaxial experiments. The diameter of the specimen was 15 times larger than the maximum size of the soil particles, satisfying the principle that the diameter of the specimen should be at least 10 times larger than the maximum size of the soil particles by the ASTM standard

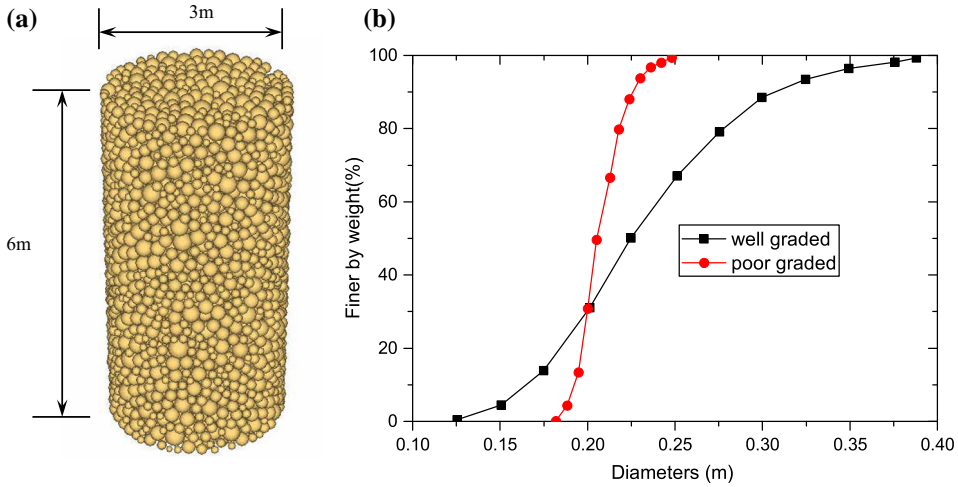

Fig. 2 **a** The schematic view and **b** the particle-size distribution of the numerical specimen

Table 1 Charateristics of the isotropically compressed specimens

Sample designation	Void ratio	Relative density	Number of particles
Medium dense	0.653	0.609	5454
Loose	0.694	0.328	5184

[5]. In order to take into account the effect of particle-size distribution, well-graded and poorly-graded specimens were analyzed in this study, as shown in Fig. 2b, but most of the numerical simulations were conducted on the well-graded specimens, and the results with the poorly-graded specimens were discussed in Sect. 4. The well-graded specimen consisted of spherical particles with diameters ranging from 0.125 to 0.388 m (the mean grain size $D_{50} = 0.225$ m), while the poorly-graded specimen consisted of spherical particles with diameters ranging from 0.182 to 0.248 m (the mean grain size $D_{50} = 0.206$ m) . The purpose of using a larger particle size was to reduce the computational time, which is determined by the square-root of the ratio of particle mass to contact stiffness. A time step $\Delta t = 8.3 \times 10^{-5}$s, which was about 1/8 of the critical time step Δt_{crit} of the system [27], was adopted in all the analyses unless stated otherwise.

Once the specimen was generated, it was compacted to the same isotropic stress state with an initial confining pressure of 400 kPa. To explore the density-dependent behavior of granular materials, the isotropically-compressed medium-dense and loose samples (Table 1) were generated. The relative density was calculated by $D_r = \frac{e_{max}-e_0}{e_{max}-e_{min}}$, where e_0, e_{max} and e_{min} are the initial void ratio, maximum void ratio and minimum void ratio of the specimen, respectively. The procedure to obtain the relative density is described as follows:

(1) Evaluating e_{max}

This procedure is modified from that proposed in Camusso and Barla [11]. The numerical procedure to determine the minimum packing state consists of generating a volume of particles and making particles fall under gravity through an opening. The numerical specimens had the same particle-size distribution and parameters used in this study. The maximum void ratio was thus obtained as $e_{max} = 0.742$.

(2) Evaluating e_{min}

First, a specimen with a relatively high void ratio (n = 0.30) was generated at the initial stage; it was equilibrated at a low confining stress (0.05 MPa) with a friction coefficient of 0.0. After that, turn the friction coefficient to 0.5, and equilibrate the specimen. The minimum void ratio was thus obtained as $e_{\min} = 0.596$.

(3) Calculating the relative density D_r.

The relative densities of the medium-dense and loose samples were 0.609 and 0.328 respectively. The medium-dense sample consisted of 5454 particles with an initial void ratio $e_0 = 0.653$, while the loose sample had 5184 particles with an initial void ratio of $e_0 = 0.694$.

After isotropic compressions, the specimens were sheared under simulated drained and undrained conditions with different rolling-friction coefficients ranging from 0.001 to 1.0. The constant confining stress test and the constant volume test are widely used to simulate the conventional triaxial test under drained and undrained conditions in DEM simulations [9,64,66]. According to classical soil mechanics, both the soil particles and pore water are incompressible, which pro-

Table 2 Parameters of used in this study

Parameters	Values
Density of ball (kg/m^3)	2700
Normal and shear stiffness of balls (N/m)	5.0e7
Normal and shear stiffness of walls (N/m)	5.0e8
Friction coefficient of between walls and balls	0.0
Friction coefficient of balls (drained test)	0.5
Friction coefficient of balls (undrained test)	0.25
Rolling-friction coefficient	0.001, 0.01, 0.02, 0.05, 0.1, 0.2, 0.3, 0.5, 1.0

vide a reasonable theoretical basis of simulating drained and undrained tests without pore water.

The triaxial shearing process was carried out by moving the top and bottom plates towards each other at a speed of 0.025 m/s, and a servo mechanism was applied to the lateral wall to maintain the confining pressure and to maintain the constant volume in the undrained tests. The parameters used in this study are shown in Table 2.

To ensure the quasi-staticity, an index I_{uf} proposed by Kuhn [34] and Ng [38] was monitored in this study. The results showed that I_{uf} remained less than 1.0%, which satisfied the quasi-static conditions in discrete-element analyses [34,38,48].

3 Numerical results

3.1 Macroscopic responses

Figure 3 shows the macroscopic responses of the specimens under simulated drained condition with different rolling-friction coefficients. The mean effective stress p' and the deviatoric stress q in triaxial compression tests are defined as $p' = (2\sigma'_r + \sigma'_z)/3$ and $q = (\sigma'_z - \sigma'_r)$, where σ'_z and σ'_r are the effective stresses along the z-direction and r-direction, respectively. As shown in Fig. 3a, both the stress ratios at the peak and residual states increased with an increase in the rolling-friction coefficient until a threshold value was attained, after which the stress ratios at the peak and residual states remained nearly identical. This trend agrees with the results in Hosn et al. [1]. Rolling resistance provided a couple of moments between two contacting particles to limit their rotations. An increase in the rolling friction led to a higher value of anti-rotation moment. The limitation of particle rotation prevented the re-distribution of particles and increased the stability of force chain during the shearing procedure. The strength increase was attributed to the increased stability of contact networks during the shearing procedure, which will be explained in Sect. 3.4. The stress ratio of the loose specimen had the same trend except that no peak state was observed (Fig. 3c). The response at small strain was basically independent of the rolling-friction coefficient in line with previous findings [29,37,44].

Figure 3b, d demonstrate the volumetric strain of the medium-dense and the loose samples versus axial strain with different rolling-friction coefficients. Similar to the stress ratios, the dilatancy increased with the rolling friction until a threshold value was attained, and it slightly decreased afterwards as shown in Fig. 3b, d. This trend also agrees with the numerical results in Hosn et al. [1].

The responses of the specimens under simulated undrained condition with different rolling-friction coefficients are presented in Fig. 4. Similar to the results in Fig. 3, the responses of undrained tests differed considerably with various values of f_r, even though the specimens had the same initial void ratio. This result is consistent with the finding in Zhao and Guo [64]. In this study, the specimen with $f_r = 0.001$ liquefied when the axial strain reached around 4.5%, while the other five specimens exhibited an obvious phase-transformation behavior, and a higher rolling friction led to a higher stability. It is noted that instability occurred for the specimens with $f_r \leq 0.05$, and the point of instability increased with an increase in the rolling-friction coefficient. After $f_r > 0.05$, the deviatoric stress continuously increased up to the ultimate strength without instable behavior. Figure 4b illustrates the evolutions of mean effective stress p' versus axial strain ε_1 for different rolling-friction coefficients. It can be seen that the mean effective stress p' was highly dependent on the rolling friction, which explains the phenomena in Fig. 4a. The responses of undrained tests were basically independent of the rolling friction when $f_r \geq 0.3$.

3.2 Effect of rolling friction on the dilatancy

Figure 5 presents the maximum dilatancy angle Ψ_{max} of the medium-dense specimens with different values of rolling-friction coefficients f_r under simulated drained conditions. The dilatancy angle is expressed as Eq. (14) based on the definition proposed by Vermeer and de Borst [57] for axisym-

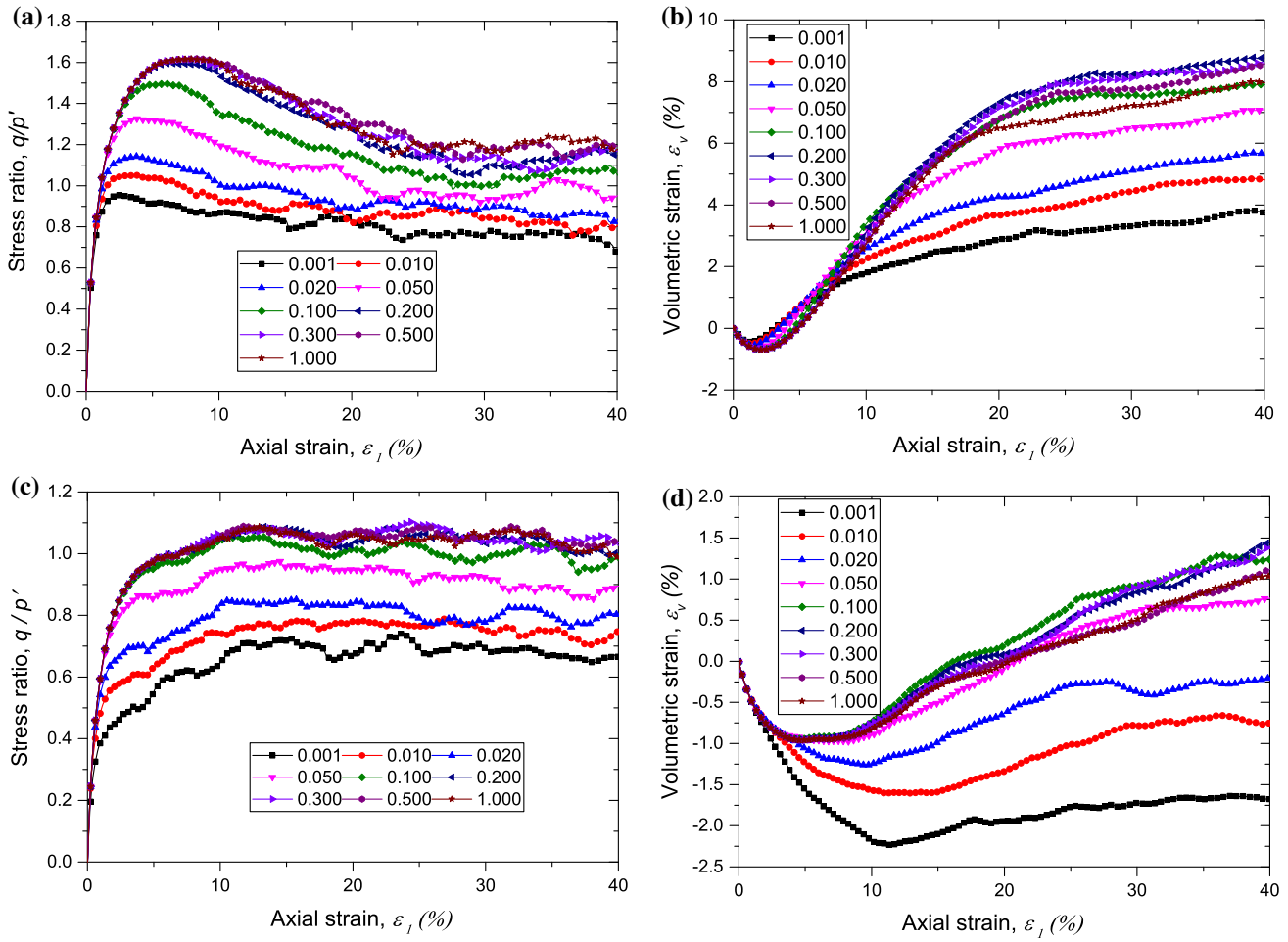

Fig. 3 Effect of rolling-friction coefficient on **a** q/p' versus ε_1; **b** ε_v versus ε_1 of medium-dense specimens and **c** q/p' versus ε_1; **d** ε_v versus ε_1 of loose specimens under drained conditions

metric and plane-strain loadings:

$$\sin \Psi = \frac{d\varepsilon_v/d\varepsilon_1}{2 - d\varepsilon_v/d\varepsilon_1} \tag{14}$$

where $d\varepsilon_v$ is the incremental volumetric strain, and $d\varepsilon_1$ is the incremental axial strain. As shown in Fig. 5, the maximum dilatancy angle increases with an increase in the rolling-friction coefficient until a certain value was attained, then the maximum dilatancy angle slightly decreased. This agrees well with the result presented by Mohamed and Gutierrez [37]. As we all know, there exists a threshold value of rolling-friction coefficient ($f_r = 0.3$ in this study), beyond which the strength remains nearly constant. Meanwhile, fewer rolling failure of contacts occurs when the threshold value of rolling-friction coefficient is reached, which will be discussed in Sect. 4. That means when $f_r > 0.3$, fewer contacts attained the rolling condition of $|M_i| \geq f_r r F_i^n$. With further increase of the rolling-friction coefficient, the particle interlocking also increased, which inhibited the redistribution of the particles. From the macro perspective, the dilatancy decreased slightly with an increase in the rolling friction when $f_r > 0.3$.

Figure 6 illustrates the stress-dilatancy relationships of the medium-dense specimens under simulated drained condition for various rolling-friction coefficients. The dilatancy index is defined as [49]

$$D = -\frac{d\varepsilon_v}{d\varepsilon_s} \tag{15}$$

where $d\varepsilon_s = 2(d\varepsilon_1 - d\varepsilon_3)/3$. As shown in Fig. 6, the stress ratio increased with D nonlinearly at a decreasing rate until the peak value was attained. A higher rolling-friction coefficient led to a higher linearity of the stress-dilatancy relationship in this stage. This is because the rotation of particles could be more strictly restrained with higher rolling-friction coefficient, which in turn caused an increasing in the stress ratio q/p' and the maximum dilatancy D_{max}. The relationships between the maximum dilatancy indices D_{max} and the associated stress ratios for all the medium-dense specimens

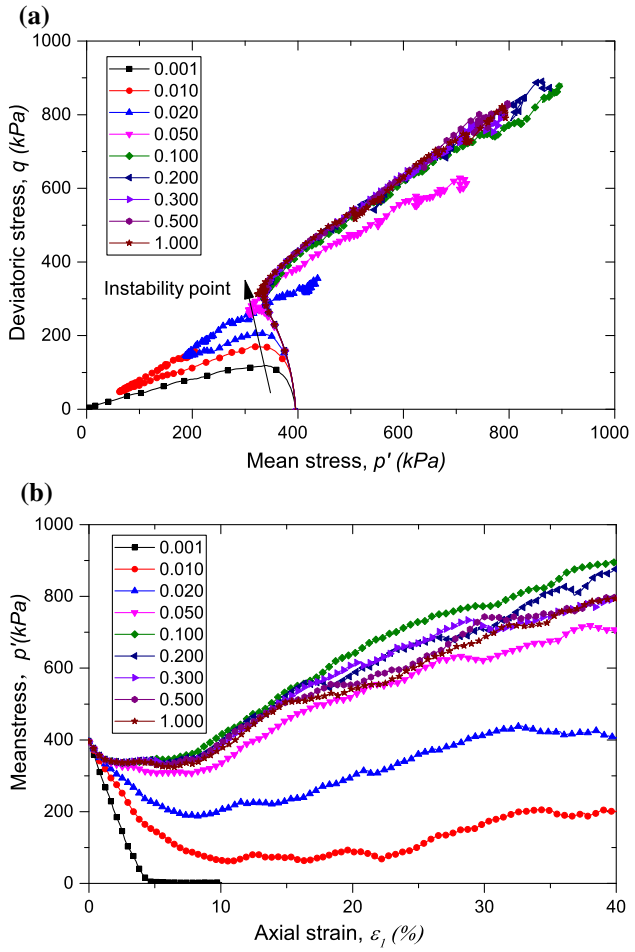

Fig. 4 Effect of rolling-friction coefficient on **a** deviatoric stress q versus mean effective stress p'; **b** mean effective stress p' versus axial strain ε_1 under undrained conditions

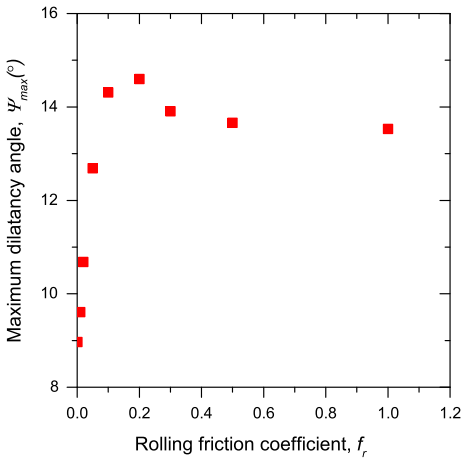

Fig. 5 Effect of rolling friction on maximum dilatancy angle $\psi_{\max}$ under drained condition

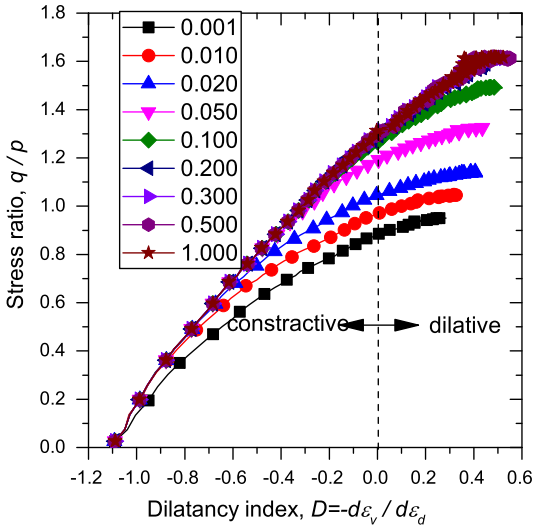

Fig. 6 Stress-dilatancy relationship with different rolling-friction coefficients under drained condtions

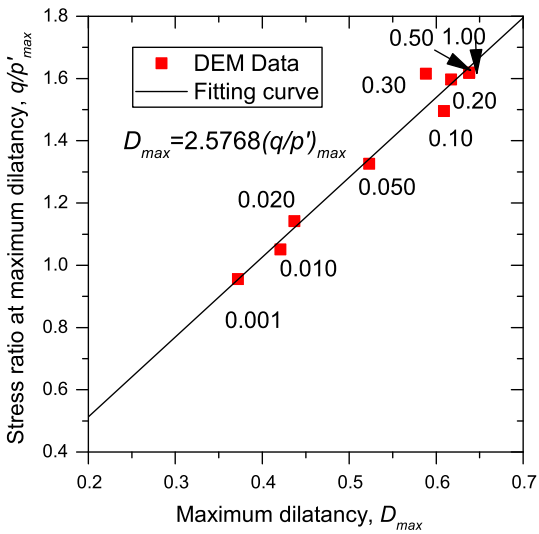

Fig. 7 Effect of rolling-friction coefficient on relationship between maximum dilatancy and stress ratio at maximum dilatancy

are illustrated in Fig. 7. It can be seen that there existed a linear relationship between the maximum dilatancy D_{max} and its associated stress ratio $\left(q/p'\right)_{max}$. Figure 8 presents the relationship between the rolling-friction coefficient f_r and the stress ratio at the state of phase transformation η_0 [26]. The value of η_0 represents the stress ratio when $D = 0$. The stress ratio at phase transformation η_0 increased considerably when the rolling-friction coefficient was less than 0.1, after which it remained nearly constant.

Previous studies showed that there existed a linear relationship between the maximum dilatancy angle Ψ_{max}, the peak friction angle ϕ_p, and the critical friction angle ϕ_{cs}

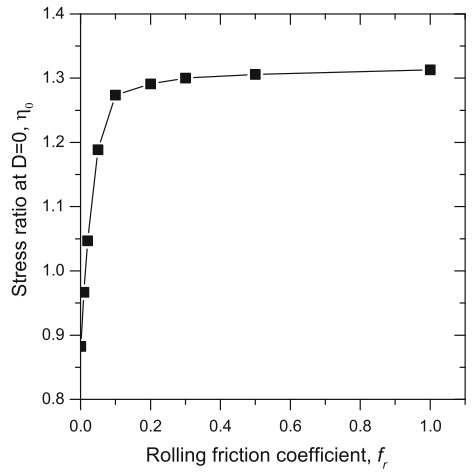

Fig. 8 Stress ratios when dilatancy index D = 0 for different rolling-friction coefficients

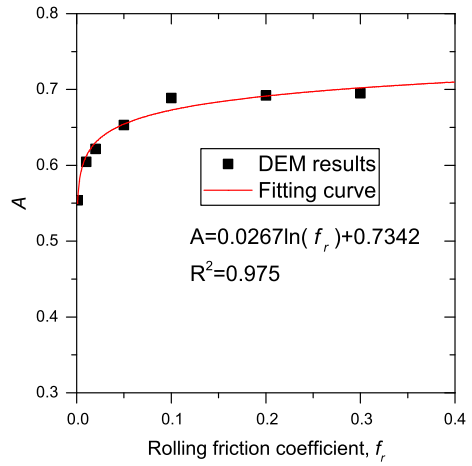

Fig. 9 Effect of rolling-friction coefficient on coefficient A

[10,13,14,17,18,23,56]:

$$\phi_p = A\Psi_{max} + \phi_{cs} \tag{16}$$

Vaid and Sasitharan [56] moved the critical friction angle ϕ_{cs} to the left side of Eq. (16), and defined an excess friction angle as:

$$\phi_{ex} = \phi_p - \phi_{cs} \tag{17}$$

This study also investigated the effect of rolling friction on the relationship between the dilatancy angle and the excess friction angle, and the result is given in Fig. 9. The dilatancy coefficient A increased with an increase in the rolling friction until $f_r = 0.2$, which implies that the coefficient A in Eq. (16) increased with the particle angularity. This is in agreement with the experimental results by Guo and Su [23]. After $f_r = 0.2$, the coefficient A remained nearly constant. It is also noted that the relationship between A and the natural logarithm of rolling-friction coefficient f_r was linear when $f_r \leq 0.2$.

3.3 Effect of rolling friction on the mechanical behavior with different inter-particle frictions

Figure 10 presents the effect of the inter-particle friction μ and rolling-friction coefficient f_r on the peak friction angle φ_p and the maximum dilation angle Ψ_{max} of the medium-dense specimens. As shown in Fig. 10, both φ_p and Ψ_{max} were significantly influenced by rolling friction when $\mu = 0.5$, while the rolling friction has little effect on φ_p and Ψ_{max} when $\mu = 0.1$. This trend agrees with the results of Zhang et al. [63].

3.4 Micro scale variables

Figure 11 shows the evolutions of the mechanical coordination number Z_m and the ratio of rattlers R_{RN} for the medium-dense and loose specimens with various rolling-friction coefficients f_r under simulated drained condition. In a granular assembly, some particles do not contribute to the force transmission [45,52], and Thornton [52] proposed the mechanical coordination number Z_m defined as:

$$Z_m = \frac{2N_c - N_1}{N_p - N_0 - N_1} \tag{18}$$

where N_c is the number of contacts; N_p is the number of particles, and N_1 and N_0 are the number of particles with 1 and 0 contacts. Figure 11a shows that Z_m decreased as the shearing deformation increased until finally attaining a constant mechanical coordination number for the medium-dense specimens. An increase in the rolling-friction coefficient led to a decrease in the value of the constant mechanical coordination number. Z_m of the loose specimens had the same trend with the medium-dense specimens except that Z_m remained nearly constant when $f_r = 0.001$ (Fig. 11c). Combined with the fact that the shear strength increased with the rolling friction shown in Fig. 3a, it can be concluded that with an increase of rolling friction, forces can be transmitted with less number of contacts, since all specimens had the same initial state, a lower value of mechanical coordinate number indicated that less contacts were engaged in the force networks. This means that the rolling friction can significantly enhance the stability of the contacting network of granular materials. The number of rattlers RN ($RN = N_0 + N_1$) represents the numbers of particles with no load-bearing capacity as defined by Barreto and O'Sullivan [8]. The ratio of rat-

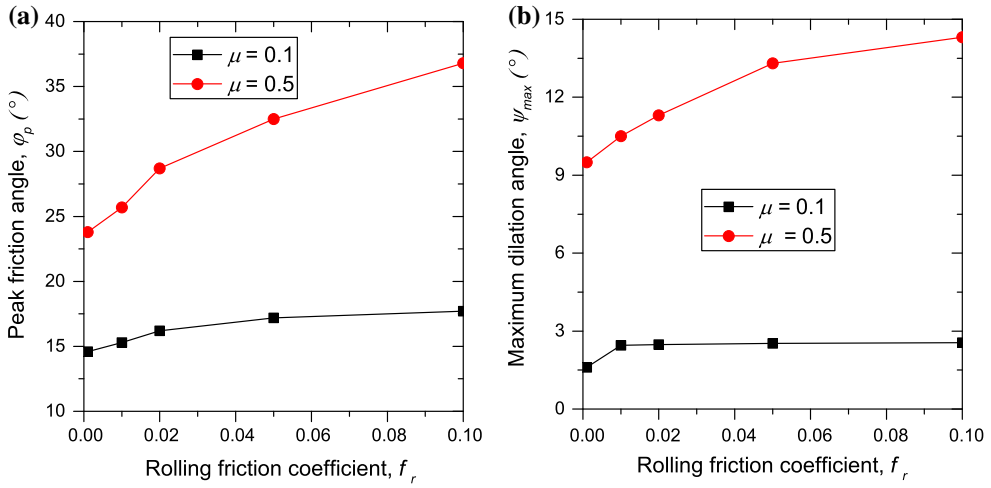

Fig. 10 Rolling friction effect on **a** the peak friction angle; **b** the maximum dilation angle

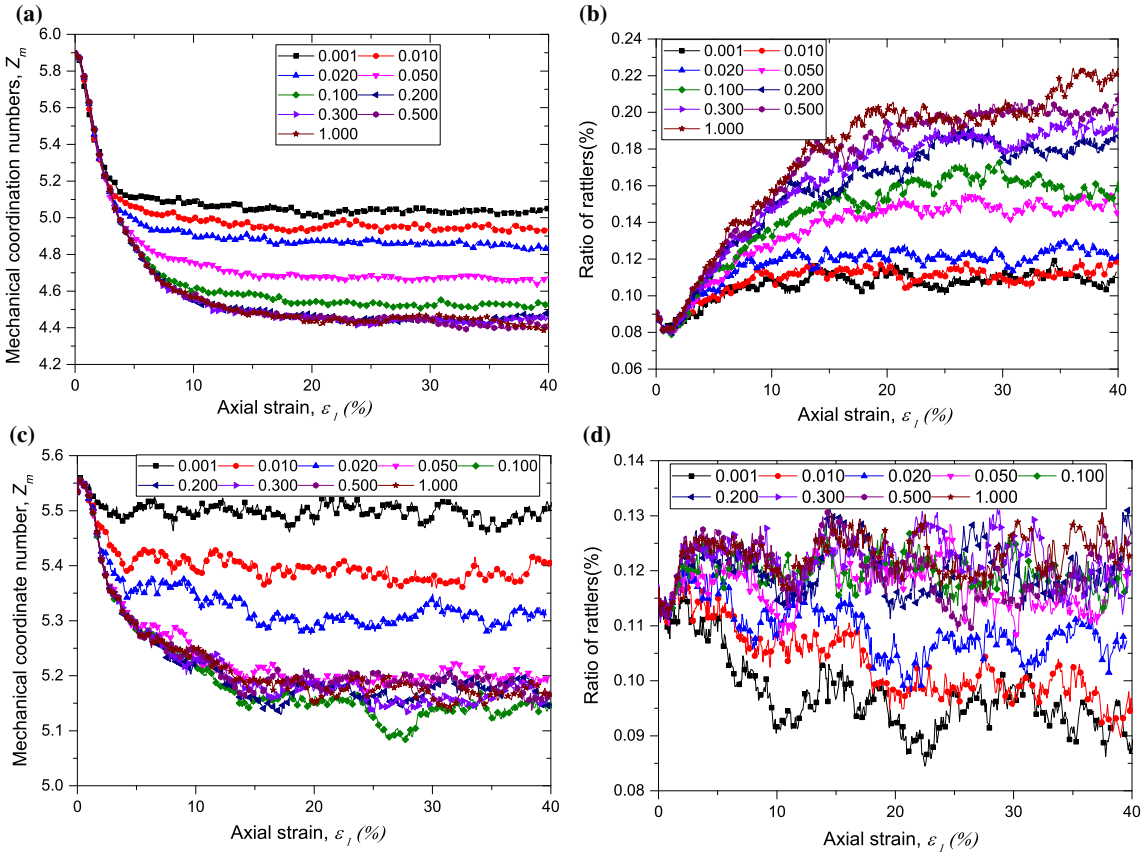

Fig. 11 Evolutions of **a** mechanical coordination number and **b** ratio of rattlers of medium-dense specimens and **c** mechanical coordination number and **d** ratio of rattlers of loose specimens under drained test condition for various rolling-friction coefficients

tlers is defined as $R_{RN} = \frac{the\ number\ of\ rattlers}{the\ number\ of\ all\ particles}$. Figure 11b, d illustrate that as the rolling-friction coefficient increased the ratio of rattlers also became larger, confirming the aforementioned conclusion on the stability of force chains. It can also be seen that the R_{RN} values reached a minimum value at around 2% of the axial strain in Fig. 11b, which is attributed to the fact that the volumetric strains of the numerical specimens in all cases reached the maximum compression at this

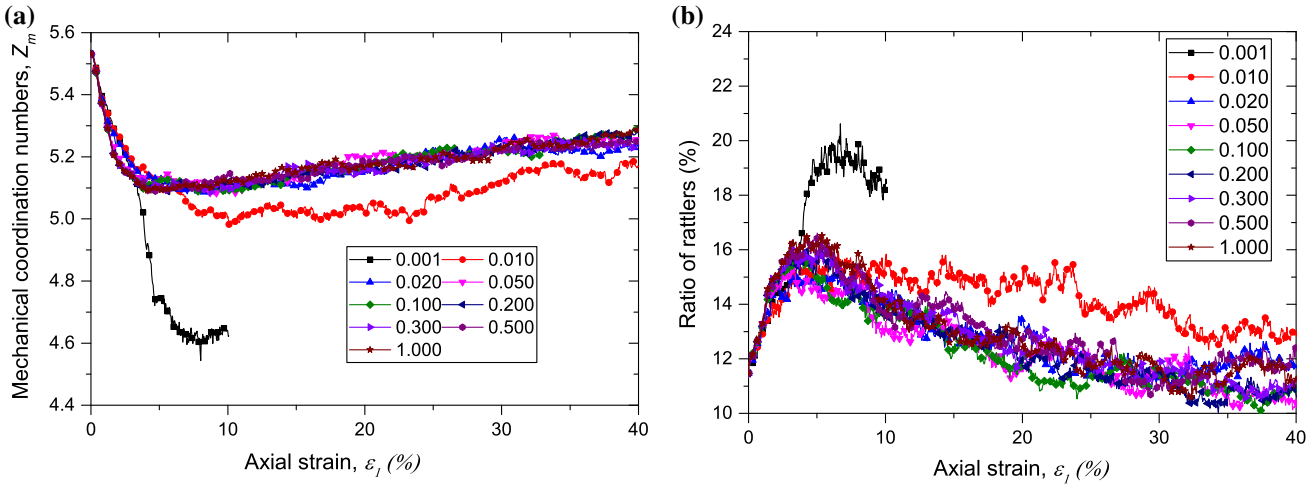

Fig. 12 Evolutions of **a** mechanical coordination number and **b** ratio of rattlers under undrained condition for various rolling-friction coefficients

axial strain as shown in Fig. 3b. The volume of the specimen decreased when the specimen was compressed, and the particles in the specimen were pushed together. Therefore some rattlers were pushed to contact with other particles, and the number of rattlers decreased. When the volumetric strain reached the maximum compression, the specimen was in the densest state, and the R_{RN} reached the minimum value.

Comparing Fig. 11a and b with c and d, the increase of dilatancy with rolling friction can be explained by the enhancement of the force-chain stability. In the dense specimens, the particles were packed in a dense state. With an increase in the shearing strain, the force chains transmitting the deviatoric stress were created, and the particles not engaging in the force transmission were pushed away in the lateral direction. Since rolling resistance can enhance the stability of the force chains, the number of particles required to transmit contact forces in the force chains decreased, and the number of particles not engaging in the force transmission increased, which led to an increase in the lateral strain. In the macroscopic scale, an increase in the rolling resistance resulted in an increase in the dilatancy for the dense specimens. In the case of the loose specimens, the force chains were prone to buckling with large initial porosities, and the particles were forced to fill the voids and to support the increasing force during shearing. With large rolling resistance, the force chains were enhanced and the initial pores were less likely to collapse, and the specimens exhibited less compression.

Figure 12 demonstrates the evolutions of the mechanical coordination number Z_m and the ratio of rattlers R_{RN} under simulated undrain condition. For the specimens with $f_r \geq 0.01$, the mechanical coordination number Z_m decreased with an increase in the axial strain until it reached nearly 4.0%, after which Z_m increased gradually; and in contrast to Z_m, R_{RN} firstly increased and then decreased gradually. For the specimen with $f_r = 0.001$, the Z_m experienced a sudden reduction when the specimen approached full liquefaction; a sudden increase of R_{RN} can also be seen. It should also be noticed that both Z_m and R_{RN} were basically independent of the rotational friction when $f_r \geq 0.02$. It is clear that the rolling friction increased the stability of the contact network, which prevented a strong contractive tendency of the packing, i.e. liquefaction. It also can be observed that there was a threshold of f_r, after which both the mechanical coordination number and the number of rattlers remained basically the same.

3.5 Macro–micro relationship

In the past few decades, many scholars have tried to establish the macro–micro relationship of granular materials [3,4,6,8,22,36,39,42,45,46,48,62,64]. Some scholars related the stress ratio to the anisotropies developed from contact normal vector, normal contact force and tangential contact force [6,22,45,46,64]; others related the stress ratio to a single parameter computed from the normal contact vector [3,4,36,39,43,48]. For example, Sazzad and Suzuki [36,48] observed that there was an unique relationship between the stress ratio and the fabric anisotropy regardless of the intermediate stress ratio and the initial density of the granular materials when strong contacts were considered. Following the methodology by Sazzard and Suzuki [48], this study investigated the effect of rolling friction on the relationship between the stress ratio and fabric anisotropy. The fabric tensor related to the unit normal vector is defined as follows [47]:

$$H_{ij} = \frac{1}{N_c}\sum_{1}^{N_c} n_i^c n_j^c \tag{19}$$

where N_c is the number of contacts and n_i^c is the i-th the component of the unit normal vector at the c-th contact.

The strong contact fabric tensor related to the unit normal vector for strong contacts is defined as follows:

$$H_{ij}^s = \frac{1}{N_s}\sum_{s\in M} n_i^s n_j^s \tag{20}$$

where M is the set of strong contacts, n_i^s is the i-th component of the unit normal vector at the s-th strong contact, and N_s the number of strong contacts.

Here a contact is considered to be a strong contact if it carries a normal contact force equal to or greater than the average normal contact force [45,53]. The average normal contact force is defined as follows:

$$f_{ave}^n = \frac{1}{N_c}\sum_{1}^{N_c} f_i^n \tag{21}$$

where f_i^n is the i-th normal contact force.

Figure 13 presents the evolutions of H_d/H_m and H_d^s/H_m^s of medium-dense specimens and H_d^s/H_m^s of loose specimens under simulated drained condition with different rolling-friction coefficients. Here H_d, H_m, H_d^s and H_m^s are defined similar to q and p [48]:

H_d is the principle deviatoric fabric at all contacts, which is defined as:

$$H_d = \sqrt{3\left\{(H_{11}-H_m)^2+(H_{22}-H_m)^2+(H_{33}-H_m)^2\right\}/2} \tag{22}$$

where $H_m = (H_{11}+H_{22}+H_{22})/3$ is the mean principal fabric at all contacts. H_d^s is the principle devietoric fabric at strong contacts, which is defined as:

$$H_d^s = \sqrt{3\left\{\left(H_{11}^s-H_m^s\right)^2+\left(H_{22}^s-H_m^s\right)^2+\left(H_{33}^s-H_m^s\right)^2\right\}/2} \tag{23}$$

where $H_m^s = (H_{11}^s+H_{22}^s+H_{33}^s)/3$ is the mean principal fabric at strong contacts.

As shown in Fig. 13a, H_d/H_m of medium-dense specimens increased with the axial strain ε_1 until ε_1 was nearly 7.5%, after which it decreased slowly to a constant value. A higher rolling-friction coefficient led to a higher value of fabric measure H_d/H_m at the same axial strain ε_1, which means that the anisotropy in contact orientation increased with an increase in the rolling friction. This result agrees well with the finding of Kuhn et al. [35]. A larger rolling friction led to a higher fabric anisotropy, indicating that the force chains required less supporting contacts in the lateral direction. It further confirmed that rolling friction can enhance the stability of the contact networks. Figure 13b shows the evolution of H_d^s/H_m^s of medium-dense specimens. The curves have the same trends as H_d/H_m but with much higher anisotropy.

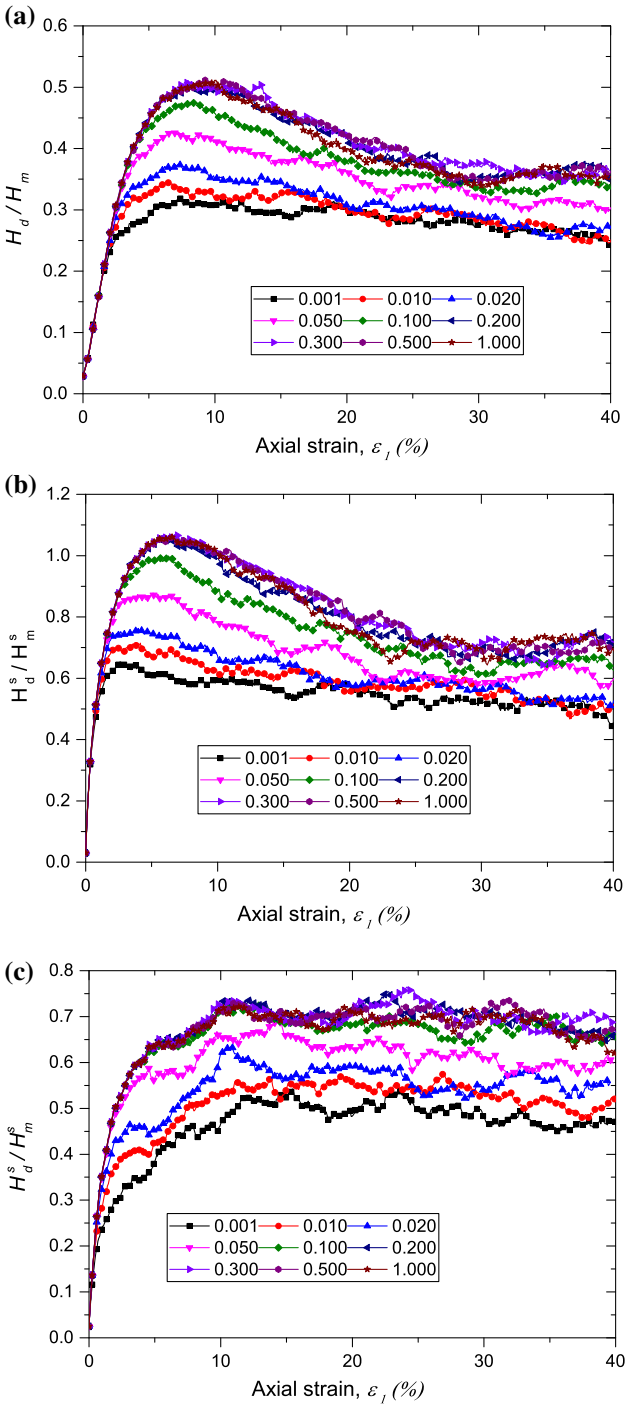

Fig. 13 The evolution of **a** H_d/H_m and **b** H_d^s/H_m^s of medium-dense specimens and **c** H_d^s/H_m^s of loose specimens versus axial strain ε_1 under drained condition

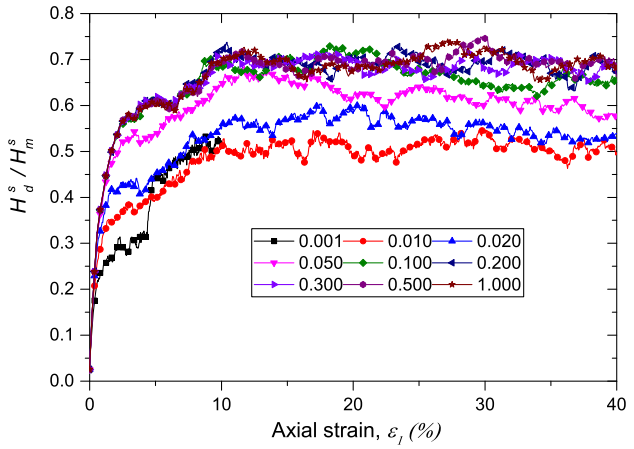

Fig. 14 The evolution of H_d^s / H_m^s versus axial strain ε_1 under undrained condition

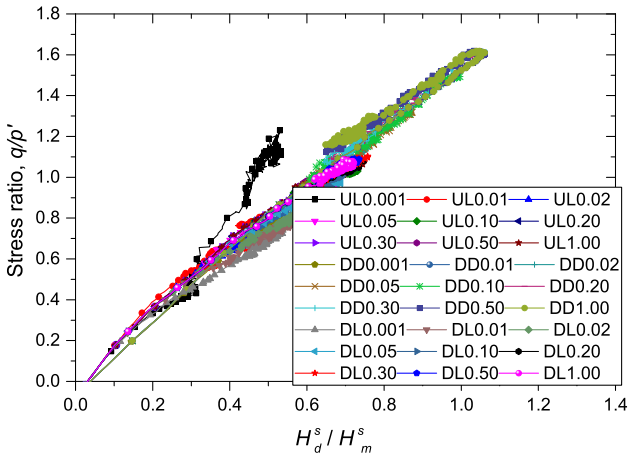

Fig. 15 Relationships between q/p' and H_d^s / H_m^s under both drained and undrained conditions

This suggests that rolling friction mainly increased the stability of strong force chains. The same conclusion can be obtained from the loose specimens under drained condition in Fig. 13c, and under undrained condition in Fig. 14.

According to previous studies, there is exists unique relationship between the stress ratio q/p' and fabric measure of strong contacts H_d^s / H_m^s regardless of the intermediate principle stress and specimen densities [36,43,48]. Figure 15 shows the relationships between the stress ratio q/p' and H_d^s / H_m^s for both medium-dense specimens and loose specimens with different rolling-friction coefficients under both simulated drained and undrained conditions (UL: undrained & loose; DD: drained & dense; DL: drained & loose). Except for the liquefied one, the relationships were almost identical, indicating that for granular materials under stable condition, drainage condition did not change the uniqueness of the macro–micro relationship. Since the specimens had different values of relative density, it can be conclude that this relationship was also independent of the relative density.

4 Discussions

In the last section, the effect of rolling-friction coefficient f_r on the stress-dilatancy behavior of granular materials has been comprehensively investigated and appropriately interpreted based on the force-chain transmitting mechanism. However, there is still one issue that has not been resolved, which is why rolling friction shows different influences on the stress-dilatancy behaviors in different studies.

As is known, the rolling resistance model has two important coefficients, one is the rolling-friction coefficient f_r and the other is the rolling stiffness parameter k_r. The stress–strain behavior of granular materials is affected by both the rolling friction and rolling stiffness. Mohamed and Gutierrez [38] and this study adopted the definition of rolling stiffness in Bardet and Huang [7] as shown Eq. (12). Hosn et al. [1] and Plassiard et al. [44] chose the following definition introduced by Iwashita and Oda [29] as

$$k_r = K^s r^2 \tag{24}$$

where K^s and r are defined by Eq. (9) and (2), respectively. The results of Hosn et al. [1] was in line with those in Mohamed and Gutierrez [37] and this study, however, the results of Plassiard et al. [44] showed that the stress-dilatancy behavior of granular materials was independent of the rolling friction.

Comparing the results of Hosn et al. [1] and Plassiard et al. [44], it can be seen that specimens in Plassiard et al. [44] had larger particle radii(0.043–0.175 m) than those in Hosn et al. [1] (0.014–0.026 m). In addition, higher initial rolling-friction coefficients ($f_r = 0.1 \sim 3.0$) were adopted in Plassiard et al. [44]. Since the value of rolling stiffness defined by Eq. (24) is related to r^2, the phenomenon in Plassiard et al. [44] may have resulted from the high values of rolling stiffness due to the large particle size when the rolling-friction coefficient exceeded a specific value. When the rolling-friction coefficient was sufficiently large, the roller might not be mobilized in the numerical tests in Plassiard et al. [44], and the dilatancy became basically independent of the rolling-friction coefficient.

For clarity, a serials of numerical drained tests with the same conditions in Sect. 3 were carried out, but the definition of rolling stiffness was defined as Eq. (24). The values of rolling stiffness in this study based on Eq. (24) and those in Plassiard et al. [44] basically had the same order of magnitude. The results presented in Fig. 16 confirm the above explanation. There was a threshold value of rolling friction. When the rolling-friction coefficient was smaller than the threshold value, it had a significant effect on the stress–strain and stress-dilatancy behaviors; however, when rolling-friction coefficient was larger than the threshold value, the stress–strain behavior was independent of

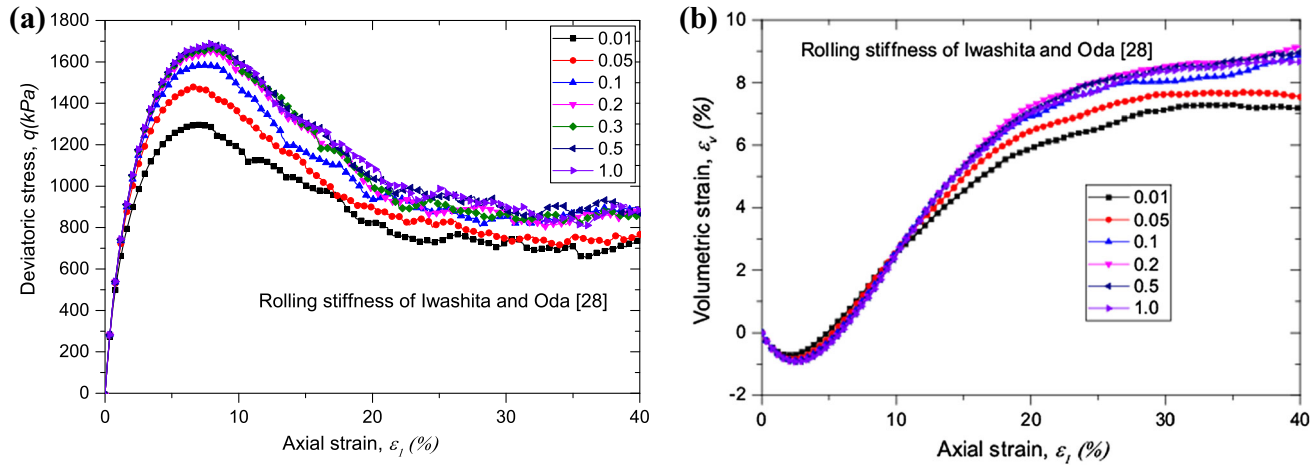

Fig. 16 Evolutions of stress–strain behaviors of granular materials with rolling stiffness of Iwashita and Oda [29]: **a** deviatoric stress q; **b** volumetric strain ε_v

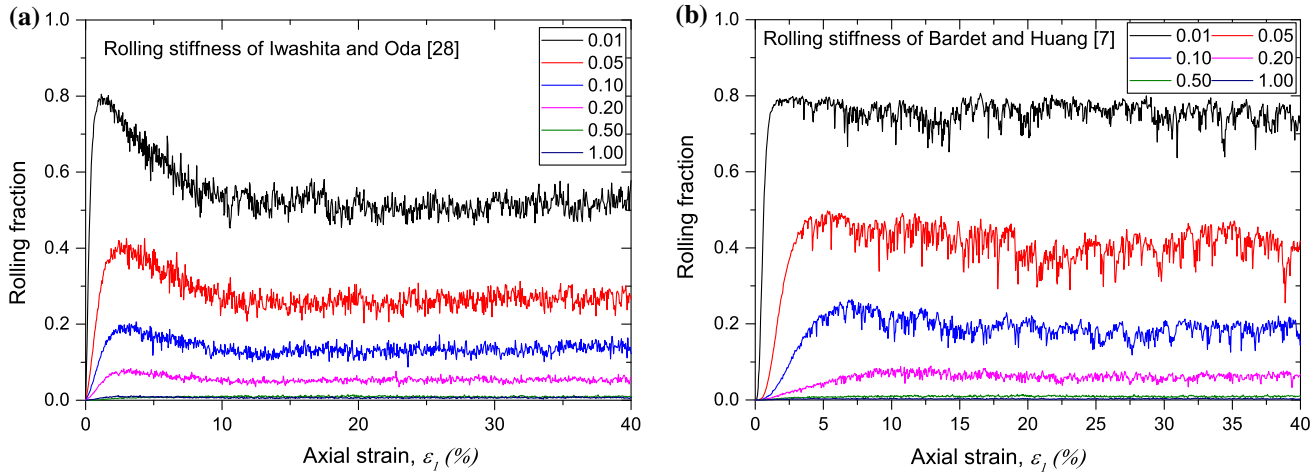

Fig. 17 Fraction of contacts with roller mobilized over different rolling-friction coefficients: **a** with rolling stiffness of Iwashita and Oda [29]; **b** with rolling stiffness of Bardet and Huang [7]

the rolling friction, and the stress-dilatancy behavior was also not affected by the rolling friction. The conclusion in Plassiard et al. [44] was obtained only because the chosen values of rolling friction were larger than the threshold value ($f_r = 0.1 \sim 3.0$). Figure 17 illustrates the evolutions of the rolling fraction for which the roller was mobilized in the contacts. The rolling fraction is defined as the ratio of rolling contacts to the total ones. Rolling is assumed to be occurred at a contact if Eq.(13) is satisfied. As shown in Fig. 17, this fraction decreased significantly with the rolling friction, and beyond some threshold value, it remained at a very small value. This means when the rolling-friction coefficient was sufficiently large, increasing the rolling friction did not influence the mechanical behavior of the numerical specimens. Comparing Figs. 3 and 15, it can also be seen that the threshold value of the rolling friction slightly decreased with an increase in the rolling stiffness.

The sensitivity of the rolling stiffness J_n on the mechanical behavior of granular materials with various f_r has also been discussed in this study. According to the rolling stiffness model proposed by Bardet and Huang [7], J_n is a dimensionless coefficient which varies theoretically from 0.25 to 0.5. Figure 18 presents the comparisons of peak friction angle φ_p and maximum dilation angle Ψ_{max} between two group of specimens with $J_n = 0.25$ and $J_n = 0.50$. The rolling stiffness J_n only influenced the specimens with a larger rolling-friciton coefficient. Both the relationship between f_r and φ_p and that between f_r and Ψ_{max} for specimens with different values of rolling stiffness had the same trend.

The effect of particle size distribution on the mechanical behavior of granular materials with different rolling frictions is also discussed. Poorly-graded specimens at medium dense state were generated and sheared under simulated drained condition. The particle size distribution of the poorly-

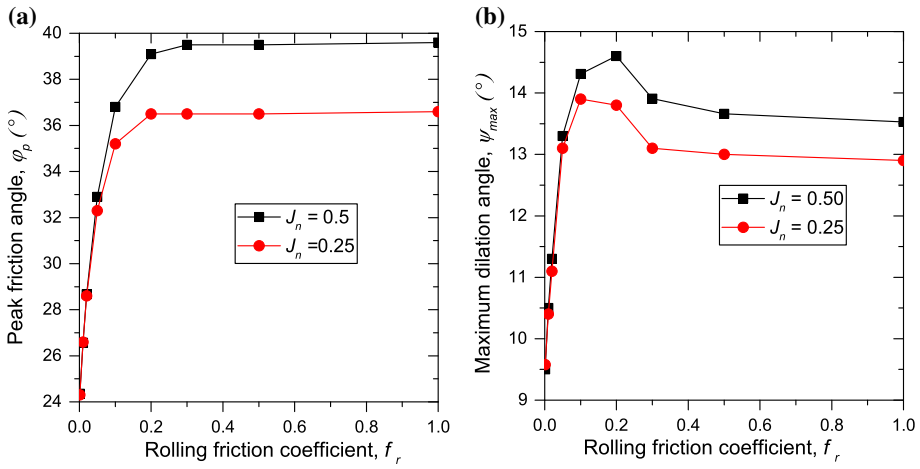

Fig. 18 The effect of J_n on the peak friction angle φ_p and maximum dilation angle Ψ_{max}

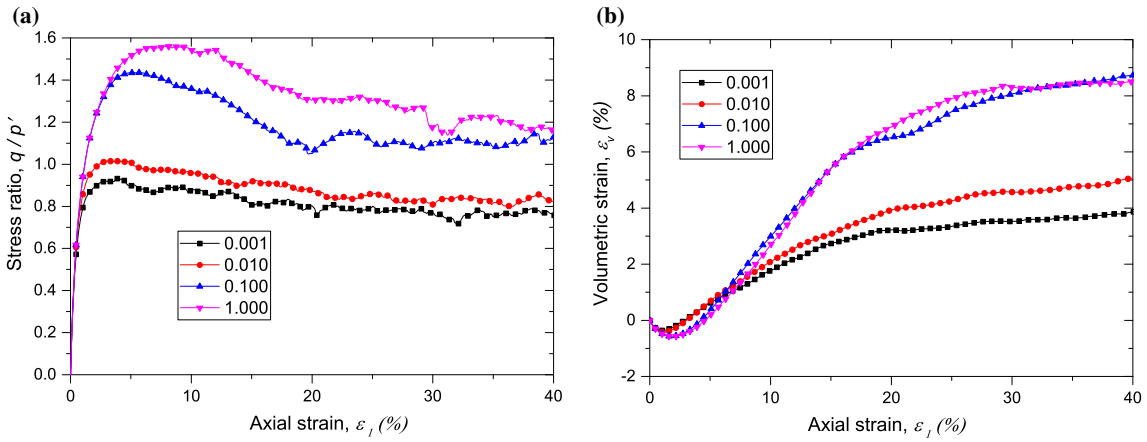

Fig. 19 The evolution of **a** stress ratio q/p and **b** volumetric strain ε_v versus axial strain ε_1 of poorly-graded specimens with various rolling-friction coefficients

graded specimens is shown in Fig. 2b. Figure 19 presents the mechanical behavior of the poorly-graded specimens with various rolling-friction coefficients. Comparing the mechanical behavior with that of the well-graded specimens (Fig. 3a, b), it can be concluded that particle grading does influence the mechanical behavior of granular materials, however the influence did not change the trend of the effect of rolling-friction coefficient on the mechanical behavior.

Another issue to be discussed is the contact model used in this study. As shown in Fig. 1, the contact model did not include the viscous terms. The viscous terms of the contact model do have significant effects on the mechanical behavior of granular materials when strain-rate effects are of interest. They influence the strength and stiffness of granular materials under different loading rates; they also influence the creep and relaxation properties. However, in this study the specimens were subjected to a monotonic loading with a very small loading velocity, and the quasi-static loading states were maintained in the analyses, as previously discussed in Sect. 2.2. The absence of the viscous terms did not change the main conclusions of this study.

In this study, the rolling resistance model has been introduced as a simple method to investigate the particle shape effect on the stress-dilatancy behavior and the relationship between macro and micro responses. However, the solid physical basis of the simple method is still not clear. Therefore, our future work will focus on finding the explicit connection between the rolling friction and a physical property of the assembly such as the particles' shape.

5 Conclusions

This study attempts to contribute to the fundamental understanding of the effect of rolling resistance on the microscopic and macroscopic responses of granular materials under both simulated drained and undrained conditions. Based on the results from numerical triaxial compression tests using DEM, the relationship between the stress-dilatancy behavior and rolling resistance was clarified. The micro-mechanical quantities were related to the macro-scale behavior by interpreting

the evolution of fabric anisotropies. The main findings drawn from this study are as follows.

1. Rolling resistance can enhance the stability of the contact network of granular materials under both drained and undrained conditions, but through different mechanisms. With a larger rolling friction, the force chains of the specimens under drained condition might be formed with a smaller number of particles and contacts, while the rolling friction could only enhance the capacity of the force transmission under undrained condition due to the limitation of volume change.
2. There existed a threshold value of rolling friction, beyond which the strength of rolling resistance was not mobilized and did not influence the mechanical behavior of granular materials. The ambiguity on the role of rolling friction on the mechanical behavior of granular materials was clarified.
3. The dilatancy of granular materials was dependent on the rolling friction. Both the maximum dilatancy angle and the dilatancy coefficient A increased with the rolling friction when it was smaller than some threshold value. A linear relationship between A and natural logarithm of the rolling-friction coefficient f_r was observed before f_r reached the threshold value. The dependence of the stress-dilatancy behavior on the rolling friction could be explained by the enhancement of the force-chain stability.
4. The relationship between the stress ratio q/p' and the fabric measure at strong contacts H_d^s/H_m^s followed a unique line, which was independent of the inter-particle friction, rolling friction and test conditions.

Acknowledgements The study was partly supported by the National Natural Foundation of China (Grant No. 51778259), which is gratefully acknowledged.

Compliance with ethical standards

Conflict of interest The authors declare that they have no conflict of interest.

References

1. Aboul Hosn, R., Sibille, L., Benahmed, N., Chareyre, B.: Discrete numerical modeling of loose soil with spherical particles and interparticle rolling friction. Granul. Matter **19**(1), 1–12 (2017)
2. Ai, J., Chen, J.F., Rotter, J.M., Ooi, J.Y.: Assessment of rolling resistance models in discrete element simulations. Powder Technol. **206**(3), 269–282 (2011). https://doi.org/10.1016/j.powtec.2010.09.030
3. Antony, S.J.: Evolution of force distribution in three-dimensional granular media. Phys. Rev. E **63**(1), 011302 (2000)
4. Antony, S.J., Kuhn, M.R.: Influence of particle shape on granular contact signatures and shear strength: new insights from simulations. Int. J. Solids Struct. **41**(21), 5863–5870 (2004)
5. ASTM: ASTM D7181: method for consolidated drained triaxial compression test for soils. In: Astm ASTM International (2011)
6. Azéma, E., Radjai, F., Saussine, G.: Quasistatic rheology, force transmission and fabric properties of a packing of irregular polyhedral particles. Mech. Mater. **41**(6), 729–741 (2009)
7. Bardet, J., Huang, Q.: Rotational stiffness of cylindrical particle contacts. Powders Grains **93**, 39–43 (1993)
8. Barreto, D., O'Sullivan, C.: The influence of inter-particle friction and the intermediate stress ratio on soil response under generalised stress conditions. Granul. Matter. **14**(4), 505–521 (2012)
9. Belheine, N., Plasslard, J.P., Donze, F.V., Darve, F., Seridi, A.: Numerical simulation of drained triaxial test using 3D discrete element modeling. Comput. Geotech. **36**(1–2), 320–331 (2009). https://doi.org/10.1016/j.compgeo.2008.02.003
10. Bolton, M.: The strength and dilatancy of sands. Geotechnique **36**(1), 65–78 (1986). https://doi.org/10.1680/geot.1986.36.1.65
11. Camusso, M., Barla, M.: Microparameters calibration for loose and cemented soil when using particle methods. Int. J. Geomech. **9**(5), 217–229 (2009)
12. Cavarretta, I., Coop, M., O'sullivan, C.: The influence of particle characteristics on the behaviour of coarse grained soils. Géotechnique **60**(6), 413–423 (2010)
13. Chakraborty, T., Salgado, R.: Dilatancy and shear strength of sand at low confining pressures. J. Geotech. Geoenviron. **136**(3), 527–532 (2010)
14. Chen, X., Zhang, J.: Influence of relative density on dilatancy of clayey sand-fouled aggregates in large-scale triaxial tests. J. Geotech. Geoenviron. Eng. **142**(10), 06016011 (2016). https://doi.org/10.1061/(ASCE)GT.1943-5606.0001542
15. Cho, G.-C., Dodds, J., Santamarina, J.C.: Particle shape effects on packing density, stiffness, and strength: natural and crushed sands. J. Geotech. Geoenviron. **132**(5), 591–602 (2006)
16. Cundall, P.A., Strack, O.D.: A discrete numerical model for granular assemblies. Geotechnique **29**(1), 47–65 (1979)
17. Dai, B.B., Yang, J., Zhou, C.Y.: Observed effects of interparticle friction and particle size on shear behavior of granular materials. Int. J. Geomech. **16**(1), 04015011 (2015)
18. Esposito III, M.P., Andrus, R.D.: Peak shear strength and dilatancy of a pleistocene age sand. J. Geotech. Geoenviron. **143**, 04016079 (2016)
19. Estrada, N., Azéma, E., Radjai, F., Taboada, A.: Identification of rolling resistance as a shape parameter in sheared granular media. Phys. Rev. E **84**(1), 011306 (2011)
20. Estrada, N., Azema, E., Radjai, F., Taboada, A.: Comparison of the effects of rolling resistance and angularity in sheared granular media. AIP Conf. Proc. **1542**, 891–894 (2013). https://doi.org/10.1063/1.4812075
21. Fityus, S., Giacomini, A., Buzzi, O.: The significance of geology for the morphology of potentially unstable rocks. Eng. Geol. **162**, 43–52 (2013)
22. Guo, N., Zhao, J.: The signature of shear-induced anisotropy in granular media. Comput. Geotech. **47**, 1–15 (2013)
23. Guo, P., Su, X.: Shear strength, interparticle locking, and dilatancy of granular materials. Can. Geotech. J. **44**(5), 579–591 (2007)
24. Guo, P.J.: Capillary interaction-induced rolling resistance between elliptical particles and its influence on grain column length at pendular state. Acta Geotech. **10**(4), 435–447 (2015). https://doi.org/10.1007/s11440-015-0368-x
25. Huang, J., Xu, S., Hu, S.: Effects of grain size and gradation on the dynamic responses of quartz sands. Int. J. Impact Eng. **59**, 1–10 (2013)
26. Ishihara, K., Tatsuoka, F., Yasuda, S.: Undrained deformation and liquefaction of sand under cyclic stresses. Soils Found. **15**(1), 15 (1975)
27. Itasca Consulting Group Inc: Particle Flow Code in 3 Dimensions, User's Guide. (1999)

28. Iwashita, K., Oda, M.: Micro-deformation mechanism of shear banding process based on modified distinct element method. Powder Technol. **109**(1–3), 192–205 (2000). https://doi.org/10.1016/S0032-5910(99)00236-3
29. Iwashita, K., Oda, M.: Rolling resistance at contacts in simulation of shear band development by DEM. J. Eng. Mech. Asce **124**(3), 285–292 (1998). https://doi.org/10.1061/(Asce)0733-9399(1998)124:3(285)
30. Jiang, M., Li, T., Shen, Z.: Fabric rates of elliptical particle assembly in monotonic and cyclic simple shear tests: a numerical study. Granul. Matter **18**(3), 1–14 (2016)
31. Jiang, M., Harris, D., Yu, H.: A unified two-dimensional contact model to capture the roughness of granular materials by rolling resistance. In: Geomechanics and Geotechnics of Particulate Media: Proceedings of the International Symposium on Geomechanics and Geotechnics of Particulate Media, Ube, Japan, 12–14 September 2006, p. 181. CRC Press (2006)
32. Jiang, M.J., Shen, Z.F., Wang, J.F.: A novel three-dimensional contact model for granulates incorporating rolling and twisting resistances. Comput. Geotech. **65**, 147–163 (2015). https://doi.org/10.1016/j.compgeo.2014.12.011
33. Jiang, M.J., Yu, H.S., Harris, D.: A novel discrete model for granular material incorporating rolling resistance. Comput. Geotech. **32**(5), 340–357 (2005). https://doi.org/10.1016/j.compgeo.2005.05.001
34. Kuhn, M.R.: OVAL and OVALPLOT: Programs for analyzing dense particle assemblies with the discrete element method (2006)
35. Kuhn, M.R., Sun, W., Wang, Q.: Stress-induced anisotropy in granular materials: fabric, stiffness, and permeability. Acta Geotech. **10**(4), 399–419 (2015)
36. Mahmud Sazzad, M., Suzuki, K., Modaressi-Farahmand-Razavi, A.: Macro–micro responses of granular materials under different b values using DEM. Int. J. Geomech. **12**(3), 220–228 (2012)
37. Mohamed, A., Gutierrez, M.: Comprehensive study of the effects of rolling resistance on the stress–strain and strain localization behavior of granular materials. Granul. Matter **12**(5), 527–541 (2010). https://doi.org/10.1007/s10035-010-0211-x
38. Ng, T.T.: Input parameters of discrete element methods. J. Eng. Mech. **132**(7), 723–729 (2006)
39. Ng, T.-T.: Macro-and micro-behaviors of granular materials under different sample preparation methods and stress paths. Int. J. Solids Struct. **41**(21), 5871–5884 (2004)
40. Nguyen, D.-H., Azéma, E., Sornay, P., Radjai, F.: Effects of shape and size polydispersity on strength properties of granular materials. Phys. Rev. E **91**(3), 032203 (2015)
41. Oda, M., Iwashita, K.: Study on couple stress and shear band development in granular media based on numerical simulation analyses. Int. J. Eng. Sci. **38**(15), 1713–1740 (2000). https://doi.org/10.1016/S0020-7225(99)00132-9
42. Pena, A., Garcia-Rojo, R., Herrmann, H.: Influence of particle shape on sheared dense granular media. Granul. Matter **9**(3–4), 279–291 (2007)
43. Phusing, D., Suzuki, K., Zaman, M.: Mechanical behavior of granular materials under continuously varying b values using DEM. Int. J. Geomech. **16**(1), 04015027 (2015)
44. Plassiard, J.-P., Belheine, N., Donzé, F.-V.: A spherical discrete element model: calibration procedure and incremental response. Granul. Matter **11**(5), 293–306 (2009)
45. Radjai, F., Wolf, D.E., Jean, M., Moreau, J.-J.: Bimodal character of stress transmission in granular packings. Phys. Rev. Lett. **80**(1), 61 (1998)
46. Rothenburg, L., Bathurst, R.J.: Analytical study of induced anisotropy in idealized granular materials. Géotechnique **39**(39), 601–14 (1990)
47. Satake, M.: Fabric tensor in granular materials. In: Proceedings of the IUTAM Symposium on Deformation and Failure of Granular materials, Delft, The Netherlands (1982)
48. Sazzad, M.M., Suzuki, K.: Density dependent macro–micro behavior of granular materials in general triaxial loading for varying intermediate principal stress using DEM. Granul. Matter **15**(5), 583–593 (2013)
49. Shen, Z., Jiang, M., Thornton, C.: DEM simulation of bonded granular material. Part I: contact model and application to cemented sand. Comput. Geotech. **75**, 192–209 (2016)
50. Sukumaran, B., Ashmawy, A.: Quantitative characterisation of the geometry of discret particles. Geotechnique **51**(7), 619–627 (2001)
51. Tang, H., Dong, Y., Chu, X., Zhang, X.: The influence of particle rolling and imperfections on the formation of shear bands in granular material. Granul. Matter **18**(1), 1–12 (2016)
52. Thornton, C.: Numerical simulations of deviatoric shear deformation of granular media. Géotechnique **50**(1), 43–53 (2000)
53. Thornton, C., Antony, S.: Quasi-static deformation of particulate media. Philos. Trans. R. Soc. London Ser. A Math. Phys. Eng. Sci. **356**(1747), 2763–2782 (1998)
54. Tordesillas, A., Walsh, D.S.: Incorporating rolling resistance and contact anisotropy in micromechanical models of granular media. Powder Technol. **124**(1), 106–111 (2002). https://doi.org/10.1016/S0032-5910(01)00490-9
55. Tsomokos, A., Georgiannou, V.: Effect of grain shape and angularity on the undrained response of fine sands. Can. Geotech. J. **47**(5), 539–551 (2010)
56. Vaid, Y., Sasitharan, S.: The strength and dilatancy of sand. Can. Geotech. J. **29**(3), 522–526 (1992)
57. Vermeer, P.A., De Borst, R.: Non-associated plasticity for soils, concrete and rock. HERON **29**(3), 1984 (1984)
58. Wang, J., Gutierrez, M.: Discrete element simulations of direct shear specimen scale effects. Géotechnique **60**(5), 395–409 (2010)
59. Wensrich, C., Katterfeld, A.: Rolling friction as a technique for modelling particle shape in DEM. Powder Technol. **217**, 409–417 (2012)
60. Wensrich, C.M., Katterfeld, A., Sugo, D.: Characterisation of the effects of particle shape using a normalised contact eccentricity. Granul. Matter **16**(3), 327–337 (2014). https://doi.org/10.1007/s10035-013-0465-1
61. Yang, J., Luo, X.: Exploring the relationship between critical state and particle shape for granular materials. J. Mech. Phys. Solids **84**, 196–213 (2015)
62. Yimsiri, S., Soga, K.: DEM analysis of soil fabric effects on behaviour of sand. Géotechnique **60**(6), 483–495 (2010)
63. Zhang, W.C., Wang, J.F., Jiang, M.J.: DEM-aided discovery of the relationship between energy dissipation and shear band formation considering the effects of particle rolling resistance. J. Geotech. Geoenviron. **139**(9), 1512–1527 (2013). https://doi.org/10.1061/(Asce)Gt.1943-5606.0000890
64. Zhao, J.D., Guo, N.: Rotational resistance and shear-induced anisotropy in granular media. Acta Mech. Solida Sin. **27**(1), 1–14 (2014)
65. Zhou, B., Huang, R.Q., Wang, H.B., Wang, J.F.: DEM investigation of particle anti-rotation effects on the micromechanical response of granular materials. Granul. Matter **15**(3), 315–26 (2013)
66. Zhou, W., Liu, J., Ma, G., Yuan, W., Chang, X.: Macroscopic and microscopic behaviors of granular materials under proportional strain path: a DEM study. Int. J. Numer. Anal. Met. **40**(18), 2450–2467 (2016). https://doi.org/10.1002/nag.2537
67. Zhou, Y.C., Wright, B.D., Yang, R.Y., Xu, B.H., Yu, A.B.: Rolling friction in the dynamic simulation of sandpile formation. Phys. A **269**(2–4), 536–553 (1999). https://doi.org/10.1016/S0378-4371(99)00183-1